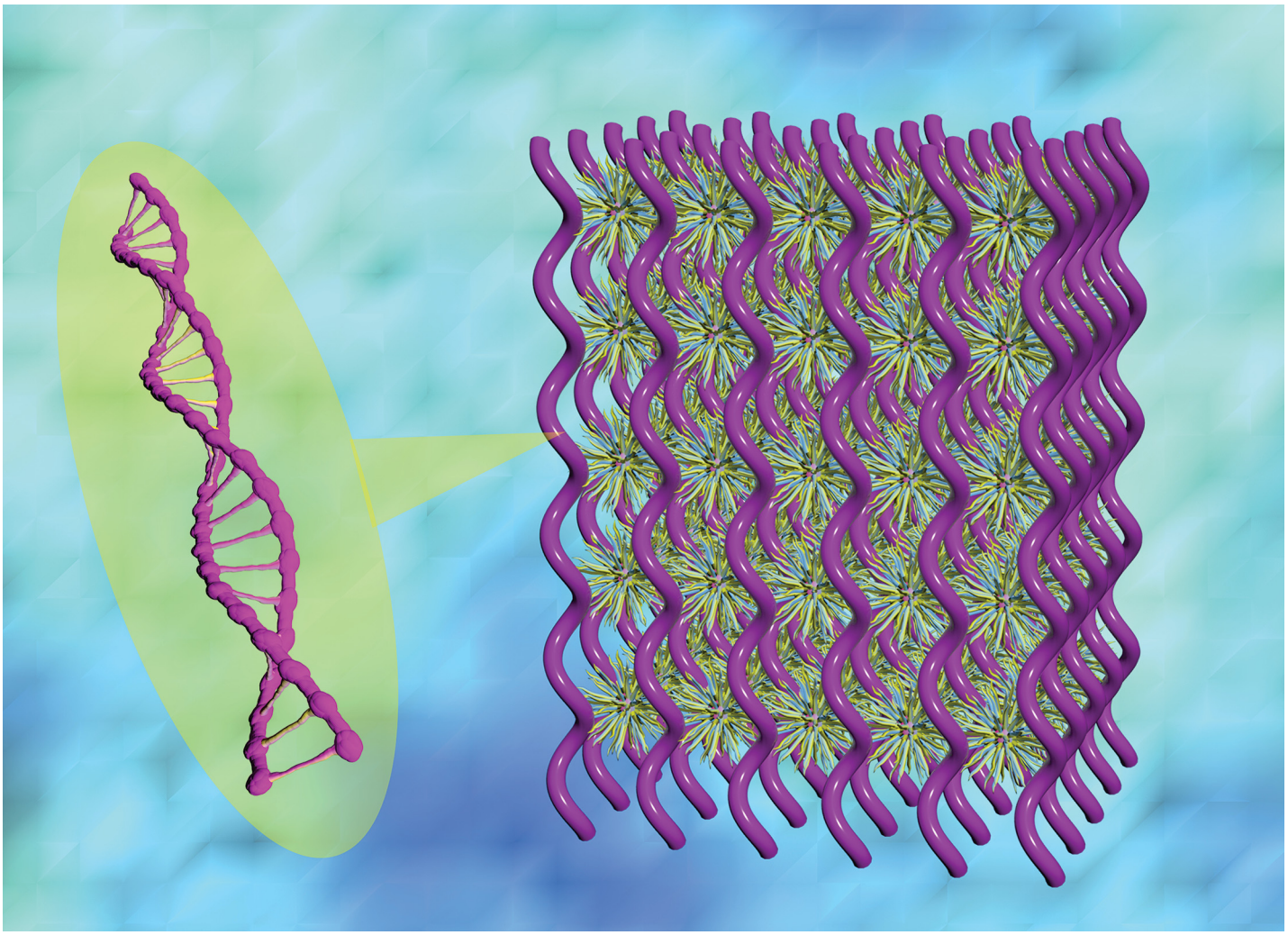

Highlighting research from the Polymer Physics Laboratory from the group of Prof. Hsin-Lung Chen.

Superhelical DNA liquid crystals from dendrimer-induced DNA compaction

A new mesophase composed of tetragonally packed DNA superhelices is studied. We study the electrostatic complex of DNA with the PAMAM G4 dendrimer using SAXS. The electrostatic attraction with the dendrimer drives the regular bending of DNA into superhelices packed in a tetragonal lattice with $P4_12_12$ symmetry, showing that the superhelices possess both identical handedness and phase conservation.

As featured in:

See Hsin-Lung Chen *et al.*, *Soft Matter*, 2021, **17**, 7287.

ROYAL SOCIETY OF CHEMISTRY

rsc.li/soft-matter-journal

Registered charity number: 207890

Soft Matter

PAPER

View Article Online
View Journal | View Issue

Published on 05 July 2021. Downloaded by National Synchrotron Radiation Research on 2/16/2022 7:10:11 AM.

Check for updates

Cite this: *Soft Matter*, 2021, **17**, 7287

Superhelical DNA liquid crystals from dendrimer-induced DNA compaction

Bradley W. Mansel,[a] Chun-Jen Su,[b] Chun-Yu Chen,[b] Chih-Mei Young,[a] Yen-Chih Huang,[a] Cheng-Che Yang[a] and Hsin-Lung Chen *[a]

Received 14th April 2021,
Accepted 5th July 2021

DOI: 10.1039/d1sm00547b

rsc.li/soft-matter-journal

Electrostatic compaction of double stranded DNA induced by a positively charged poly(amidoamine) (PAMAM) dendrimer of generation four (G4) was found to produce two unique types of DNA mesophases, in which the DNA bent into superhelices packed in a tetragonal or hexagonal lattice. The structure formed at a lower dendrimer charge density was three-dimensionally (3D) ordered, as characterized by the $P4_12_12$ space group with a 4_1 screw axis in a tetragonal arrangement, showing that the weakly bent DNA superhelices with a pitch length of *ca.* 5.0 nm possessed both identical handedness and phase conservation. The 3D ordered structure transformed into a 2D mesophase at a higher dendrimer charge density, wherein the strongly bent superhelices with a pitch length of *ca.* 4.0 nm organized in a hexagonal lattice without lateral coherence of helical trajectory. The counterion valency of the protonic acid that is used to charge the dendrimer was found to influence the phase diagram. Under a given dendrimer charge density, the complex with a multivalent acid-protonated dendrimer tended to form structures with less curved DNA, attesting that the driving force of charge matching was reduced by increasing the counterion valency of the dendrimer.

Introduction

Understanding the non-covalent self-assembly of charged species is an important problem, not only for developing a broad range of industrially relevant materials, but also for understanding the origin of life.[1] The interaction between charged species is highly complex, due to the strong electrostatic interactions that polyions exhibit and the large length scales over which they persist.[2] Such mechanisms, which are often exploited by nature to assemble complex functional structures, also involve entropic effects not only from polyions, but also from counterions and co-ions as well as water. The delicate interplay among the enthalpic and entropic components of free energy has been shown to produce a number of structures with high levels of complexity.[3,4]

Double stranded DNA possesses a number of physical properties pertinent to its compaction and self-assembly into a plethora of biologically relevant structures.[5,6] While the DNA double helix structure was discovered back in the 1950s,[7–9] investigations into DNA self-assembly are ongoing.[10–12] The high linear charge density and a complex helical structure centered on hydrogen bonding between the two complementary chains allow the introduction of a number of self-assembly mechanisms and a great number of minimum free energy structures.[13–16] Many structures are highly relevant to biological systems and are key for further understanding of how long DNA strands are packaged to fit into cells.[17–19] Furthermore, DNA compaction holds significant importance for the delivery of genetic materials in gene therapy.[20]

DNA can be compacted through a number of different mechanisms which typically involve an external compacting agent.[21] The external compound shifts the free energy minimum of the system from that of globally disordered coils to an ordered condensed DNA phase.[21] Different compacting agents can produce a range of structures by imparting mechanical or electrostatic forces. For instance, the introduction of polycations, such as polyamines possessing a charge of +3 or greater, can spontaneously condense DNA into toroids or rods *in vitro*.[22–24] While such a compaction mechanism alone has not been identified in biological systems, polyamines also are likely to play an important role in the final stages of DNA ejection from phages.[25]

Superhelices and supercoils are other intriguing structures found in compacted DNA. The plasmid DNA in prokaryotic cells is enzymatically over or under the wound, resulting in supercoiled plasmids for efficient intracellular packing.[26,27] The compaction of DNA with larger globular polycations, such as proteins *in vivo* or polymers[28] and micelles[29] *in vitro*, through electrostatic attraction perpendicular to the DNA helical axis offers another effective route to bend DNA into a superhelix or supercoil. If such forces are sufficiently large to outweigh the energetic cost to bend DNA across the radius of curvature of the

[a] *Department of Chemical Engineering, National Tsing Hua University, Hsinchu 30013, Taiwan. E-mail: hlchen@che.nthu.edu.tw*
[b] *National Synchrotron Radiation Research Center, Hsinchu 300, Taiwan*

Published on 05 July 2021. Downloaded by National Synchrotron Radiation Research on 2/16/2022 7:10:11 AM.

globular polyanion, DNA can wrap around its surface to form a superhelix. Such a mechanism is found in the DNA compaction in eukaryotes, where the genetic DNA wraps helically around globular histone proteins *via* electrostatic interaction in nucleosome core particles, leading to the chromatin fiber that successively folds into a highly compact entity for fitting into the limited space of the cell nucleus.

Cationic poly(amidoamine) (PAMAM) dendrimers are a class of globular polycations that have been used to generate a range of condensed DNA phases through electrostatic complexation.[3,30] These hyperbranched polymeric molecules are typically grown radially by a layer-by-layer method from a central core with the number of layers termed the generation number, G*n*, with *n* being the total number of layers. PAMAM dendrimers are of great interest for DNA compaction due to their biocompatibility and well-defined size which varies from 1.5 to 13 nm as the generation number increases from zero to eleven. The charge of the PAMAM dendrimer can be systematically varied through the protonation state, which is quantified through the degree of protonation (dp) defined as the number fraction of protonated amine groups. The electrostatic complexes of DNA with dendrimers (called "dendriplexes") have drawn significant attention for developing effective nonviral gene vectors. Moreover, considering the geometric similarity between the dendrimers of intermediate generations and the histone proteins, the dendriplex may also be considered as a synthetic model system for understanding the interaction between the DNA and histone in a nucleosome and the associated self-organization behavior of the nucleosome or chromatin.[31,32]

Recent investigations have disclosed a number of novel ordered phases for the dendriplex, where both the size and charge of the dendrimer were found to be crucial in determining the resultant structure. With an increasing charge and generation number of the PAMAM dendrimer, the dendriplex was found to exhibit a higher propensity to form structures with curved DNA due to the stronger driving force of charge matching and the lower energetic penalty for bending DNA. At one extreme, DNA wrapped dramatically around the dendrimers of intermediate to high generation ($\geq$G4) above the generation-dependent threshold dendrimer charge density, yielding a nucleosome-like structure.[33,34] At the other extreme of low dendrimer charge density and low generation number ($\leq$G4), the dendriplexes formed a columnar mesophase with locally straight DNA packed in 2D hexagonal ($\leq$G3) or square (G3 and G4) lattices.[34,35] A unique mesophase composed of DNA bent moderately into the superhelices organized in a hexagonal lattice was identified in complexes with a PAMAM G4 dendrimer with an intermediate dp.[34] The work of Dootz *et al.* on dendriplexes with a PAMAM G6 dendrimer has revealed the formation of a 3D body-centered orthorhombic phase in which the DNA was proposed to curve coherently in the lattice.[36] These studies demonstrate that the PAMAM dendrimer can bend DNA to different degrees to produce the mesophases composed of DNA superhelices organized in well-defined lattices.

Using small angle X-ray scattering (SAXS) together with real-space modeling, here we demonstrate the bending of DNA by a PAMAM G4 dendrimer into superhelices with two distinct states, yielding DNA liquid crystals with two- and three-dimensional orders. In particular, we disclose a novel three-dimensionally (3D) ordered DNA mesophase characterized by the $P4_12_12$ space group with the weakly bent DNA superhelices arranged in a tetragonal lattice. The conservation of the helical phase was however lost as the dendrimer charge density was increased above a threshold value, transforming the 3D superhelical mesophase into the 2D hexagonal superhelical mesophase disclosed previously. We further examined the effect of counterion valency of the protonic acid that is used to charge the dendrimer on the phase window of the superhelical mesophases. It was observed that the dendriplex with a multivalent acid-protonated dendrimer tended to form a structure with less curved DNA. The observed valency effect was rationalized by the stronger electrostatic attraction between multivalent counterions and dendrimers coupled with less entropic gain from the counterion release.

Experimental section

Materials and preparation of dendriplexes

Sample preparation was performed at room temperature (*ca.* 25 °C). Initial stock solutions of DNA were prepared by dissolving calf thymus DNA acquired from Sigma Aldrich in ultrapure water (18.2 MΩ) to a concentration of 3 mg ml^{-1}. Stock PAMAM G4 dendrimer solutions were made by diluting the 100 mg ml^{-1} aqueous solutions obtained from Dendritech Inc. to 3.5 mg ml^{-1}. The dendrimer was protonated by 0.1 N $HCl_{(aq)}$ or 0.1 N multivalent protonic acids including H_2SO_4 and H_3PO_4 to the prescribed degree of protonation (dp), which signifies the number fraction of protonated amine groups in the dendrimer. The dp values of the dendrimer were confirmed by the pH measurement. The sample preparation resulted in negligible changes to the ionic condition with a maximum difference of few tens of mM.

The protonated dendrimer solution was titrated into the Calf thymus DNA aqueous solution (with a DNA concentration of 2 mg ml^{-1}) to reach the designated nominal N/P ratio, $(N/P)_n$, for forming the dendriplex precipitate suspended in aqueous medium. The nominal N/P ratio stands for the feed molar ratio of the amine group of the dendrimer to the phosphate group of DNA. It is noted that at the highest dp value (= 0.9) of the dendrimer studied, the pH was *ca.* 5.5 which is far above the pK_a (= 2) of the DNA phosphate groups; consequently, the groups remained unprotonated and charged under all experimental conditions accessed. The dendriplexes with an $(N/P)_n$ of 6.0 were prepared here. The samples were equilibrated at room temperature for 72 hours prior to undertaking the structural characterization experiments to ensure structural equilibration.

Small angle X-ray scattering (SAXS)

SAXS experiments were carried out at the National Synchrotron Radiation Research Center (NSRRC) located at Hsinchu, Taiwan, using a PILATUS 1M detector on the BL23A SWAXS beamline at a wavelength λ of 0.1240 nm and a sample-to-detector distance of 3 m. Such a configuration gave rise to a scattering vector,

 This journal is © The Royal Society of Chemistry 2021

Published on 05 July 2021. Downloaded by National Synchrotron Radiation Research on 2/16/2022 7:10:11 AM.

$q = 4\pi\lambda^{-1}\sin(\theta/2)$, of 0.007–0.5 Å^{-1}, where θ is the angle between the incident and scattered radiation. The collected scattering patterns were radially averaged to obtain one-dimensional scattering intensity profiles. All the scattering profiles were corrected for the scatterings from air and cells. The dendriplex samples in the form of precipitates suspended in water were sealed in the cell with Kapton windows for the SAXS measurements. The amount of water in the cell was in large excess of that of complex precipitates to ensure that the water content in the complex reached saturation.

Results and discussion

Fig. 1(a) shows the SAXS profiles of the dendriplexes prepared with HCl-protonated dendrimers as a function of dendrimer dp. Here we further present the scattering profiles of the dendriplexes prepared with the dendrimers protonated by the multivalent protonic acids, including sulfuric acid and phosphoric acid, as displayed in Fig. 1(b) and (c). Since the X-ray scattering length density (SLD) contrast of DNA relative to water is about 2.8 times that of the PAMAM dendrimer, the SAXS intensity profile would reveal mainly the structure of DNA in the dendriplex.[31] Three types of SAXS patterns relevant to the DNA mesophase were discerned from Fig. 1. The Type I SAXS profile observed at a low dp shows the diffraction peaks with a position ratio of $1:2^{1/2}:4^{1/2}$, which is a characteristic scattering pattern of the square columnar (SQ) phase wherein the locally straight DNA columns packed in a 2D square lattice with a lattice parameter of 4.1 nm.

The Type II profile was observed in the regime of high dendrimer charge density and it exhibits two sharper peaks with the position ratio of $1:3^{1/2}$ and a broad halo (denoted as "q_P") situated between them. This scattering pattern was assigned to the hexagonally packed DNA superhelix phase (HEX_h), in which DNA bent into the superhelices organized in a hexagonal lattice.[34] The facts that there were no other sharp diffraction peaks and the q_p peak was broad imply that the lattice was not 3D ordered. In other words, the helical trajectories of the superhelices were not in phase, where the grooves of the superhelices shifted randomly along their long axis (*i.e.*, z axis) with respect to a reference superhelix, as schematically illustrated in Fig. 2(a).

Attempts were made to calculate the powder patterns of the HEX_h structure for comparison with the experimentally observed SAXS profiles using the real-space model. We constructed a hexagonal lattice composed of DNA superhelices represented by helical cylinders with a diameter of 2 nm.[34] The G4 dendrimer molecules (represented by spheres with a diameter of 4 nm) were placed in the tunnel regions between DNAs in such a way that there existed a characteristic interparticle distance along the z axis, as shown in Fig. 2(a). All DNA chains were assumed to be right-handed superhelices characterized by the pitch length P and the helix radius R_h defined as the radial distance between the centerline and the central trace of the helix ($R_h = 0$ for completely straight DNA).[31] To place the DNA superhelices in the lattice, we assigned the maximum value of shift distance $D_{s,max}$, and each superhelix was shifted by a distance chosen randomly between 0 and $\pm D_{s,max}$ along the z axis with respect to a reference helix, such that the superhelices in the hexagonal lattice were not all in phase.

The system with the constructed structure was then divided into numerous cubic volume elements (each has a volume of $0.5 \times 0.5 \times 0.5$ nm^3) and the partial structure factors associated

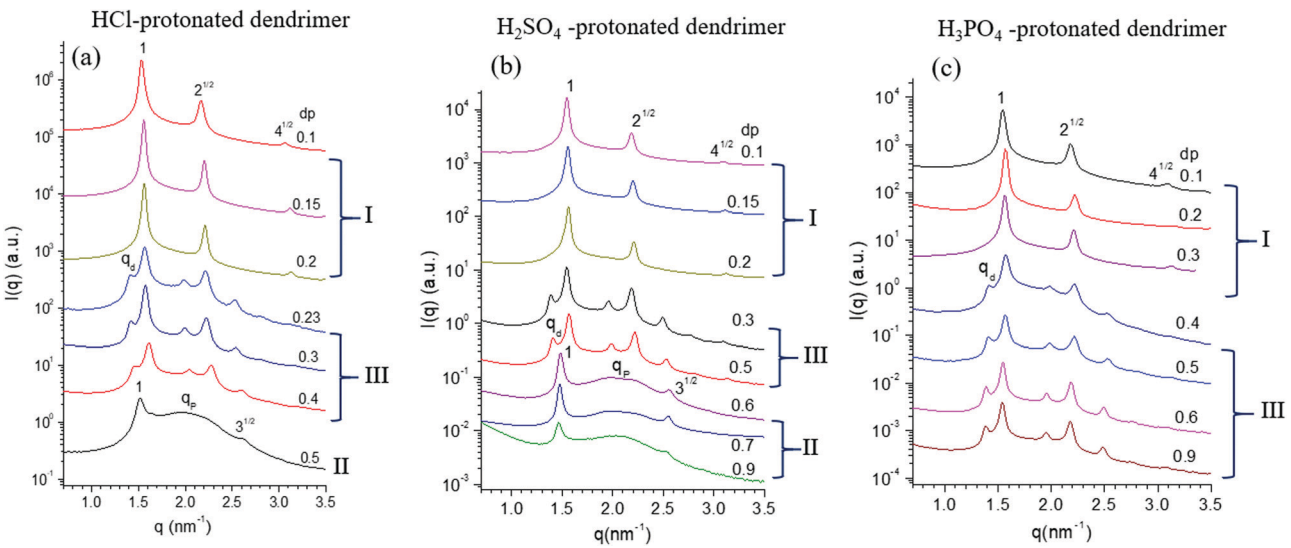

Fig. 1 The SAXS profiles of the dendriplexes prepared with (a) HCl-protonated dendrimers, (b) H_2SO_4-protonated dendrimers, and (c) H_3PO_4-protonated dendrimers as a function of the degree of protonation (dp) of dendrimer. Three types of scattering patterns denoted as I, II, and III are identified. The Type I pattern is associated with the square columnar phase (SQ) of DNA. The Type II pattern showing a broad peak (marked by q_p) situating between two peaks showing the position ratio of $1:3^{1/2}$ is assigned to a hexagonally packed DNA superhelix phase (HEX_h) with q_p being the form factor maximum of the highly bent DNA superhelix. The Type III pattern is assigned to a 3D ordered tetragonally DNA superhelix phase ($TETRA_h$) characterized by the $P4_12_12$ symmetry and weaker bending of DNA. The peak denoted by q_d is associated with the characteristic interparticle distance of the dendrimers accommodated in the lattice.

Published on 05 July 2021. Downloaded by National Synchrotron Radiation Research on 2/16/2022 7:10:11 AM.

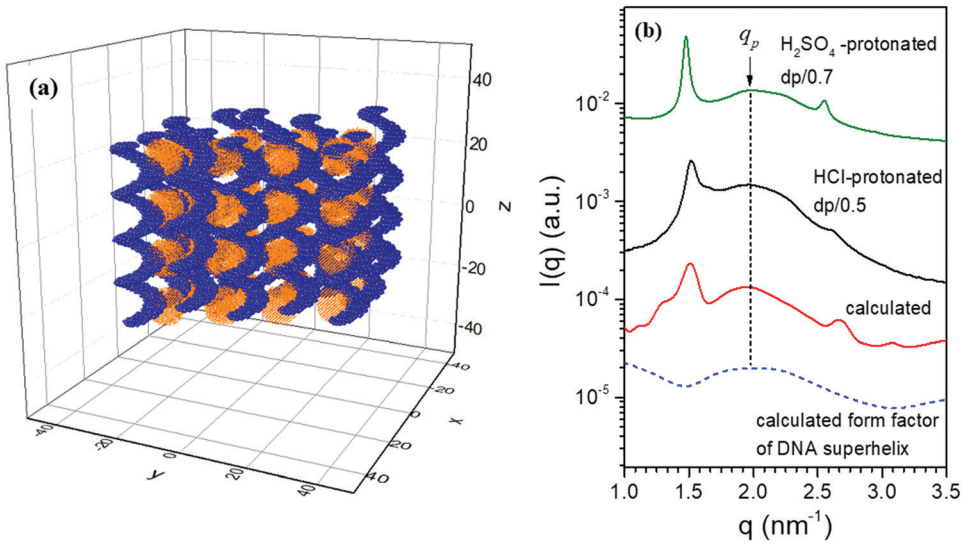

Fig. 2 (a)The real-space model constructed for calculating the SAXS profile of the HEX_h phase using the Debye equation. DNA superhelices are represented by right-handed helical cylinders with a diameter of 2 nm. Each helix has a random phase. Dark yellow spheres represent the dendrimer. (b) Comparison between the calculated SAXS curve (red) of the HEX_h phase with the experimentally observed scattering profiles. It can be seen that the agreement is good. The broad q_p peak corresponds to the form factor maximum of the superhelix, as demonstrated by the calculated form factor curve (dashed curve) of a single superhelix.

with the DNA–DNA correlation $S_{DD}(q)$, DNA–dendrimer correlation $S_{Dd}(q)$, and dendrimer–dendrimer correlation $S_{dd}(q)$ were calculated by the Debye equation, *viz.*[37,38]

$$S_{dd}(q) = \sum_{i\in G4}\sum_{j\in G4}\frac{\sin(q|\boldsymbol{r}_i - \boldsymbol{r}_j|)}{q|\boldsymbol{r}_i - \boldsymbol{r}_j|} \quad (1)$$

$$S_{DD}(q) = \sum_{i\in DNA}\sum_{j\in DNA}\frac{\sin(q|\boldsymbol{r}_i - \boldsymbol{r}_j|)}{q|\boldsymbol{r}_i - \boldsymbol{r}_j|} \quad (2)$$

$$S_{Dd}(q) = \sum_{i\in DNA}\sum_{j\in G4}\frac{\sin(q|\boldsymbol{r}_i - \boldsymbol{r}_j|)}{q|\boldsymbol{r}_i - \boldsymbol{r}_j|} \quad (3)$$

where $|\boldsymbol{r}_i - \boldsymbol{r}_j|$ is the distance between volume elements i and j in the model.[31] The SAXS intensity was then obtained from the three partial structure factors by the following equation,[31]

$$I(q) = \Delta\rho_{DNA}{}^2 S_{DD}(q) + 2\Delta\rho_{DNA}\Delta\rho_{den}S_{Dd}(q) + \Delta\rho_{den}{}^2 S_{dd}(q) \quad (4)$$

where $\Delta\rho_{DNA}$ and $\Delta\rho_{den}$ are the X-ray scattering SLD of the DNA and dendrimer, respectively. $\Delta\rho_{DNA}$ was taken as $2.85\Delta\rho_{den}$ for the calculation.[31]

Fig. 2(b) displays the calculated SAXS curve of the HEX_h structure constructed with the following parameter values: lattice parameter D_{10} = 4.7 nm, P = 4.0 nm, R_h = 1.3 nm, the number of unit cells = 7, and the number of helical turns = 4. It can be seen that the calculated scattering curve and the experimentally observed profiles showed good agreement. The broad q_p peak corresponded to the form factor maximum of the superhelix, as demonstrated in Fig. 2(b) which also shows the calculated form factor curve of a single superhelix. The intensity of this peak relative to the (10) peak decreased with a decreasing R_h; moreover, its position was determined by the pitch length of the superhelix, where the peak shifted to a lower q with the increase of the pitch length.

The Type III profile was identified at dendrimer charge densities lying between those associated with SQ and HEX_h phases. This scattering pattern contained six sharp diffraction peaks and was attributed to the superposition of the scattering peaks of SQ and HEX_h phases in our previous study.[34] However, a comprehensive survey of Type III profiles displayed by the dendriplexes prepared under different conditions revealed that the relative peak intensities were highly reproducible. For instance, the Type III profiles displayed in Fig. 1 were virtually identical irrespective of the dendrimer charge density and the counterion valency of the protonic acid used for dendrimer protonation. If this scattering pattern arose from the coexistence of SQ and HEX_h phases, the proportion and hence the relative peak intensities associated with these two phases should have varied with the preparation condition. Consequently, the Type III profile should stem from a well-defined ordered structure.

A detailed examination of the peak positions of the Type III profile revealed that, except for the first peak denoted as q_d, all diffraction peaks can be indexed according to a tetragonal unit cell with the $P4_12_12$ space group and the unit cell dimension a = b = 4.06 nm and c = 5.10 nm, as shown in Fig. 3(a). $P4_12_12$ is a space group with a 4_1 screw axis and tetragonal arrangement of the polymer chains;[39] therefore, the structure giving rise to the Type III SAXS profile was three-dimensionally ordered, with DNA adopting the superhelical conformation organized in a tetragonal lattice. This structure was denoted as $TETRA_h$. In contrast to the HEX_h phase, the helical trajectories of the DNA superhelices in $TETRA_h$ were in phase, as schematically illustrated in Fig. 3(b). Moreover, the fact that the broad form factor halo of the superhelix was not discernible in the Type III pattern suggested that the R_h of the helix was small due to relatively weak bending.

 This journal is © The Royal Society of Chemistry 2021

Published on 05 July 2021. Downloaded by National Synchrotron Radiation Research on 2/16/2022 7:10:11 AM.

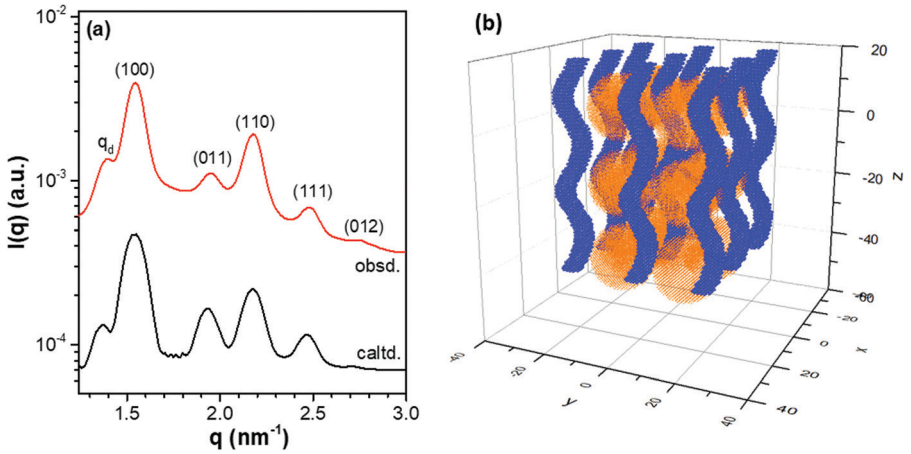

Fig. 3 (a) A representative Type III SAXS profile, showing that the diffraction peaks can be indexed according to a tetragonal unit cell with the $P4_12_12$ space group and the unit cell dimensions $a = b = 4.06$ nm and $c = 5.10$ nm except for the peak marked by q_d. The corresponding structure is a 3D ordered tetragonally packed DNA superhelix phase ($TETRA_h$). The figure also shows the calculated SAXS curve (black) of the $TETRA_h$ phase using the real-space model displayed in (b). It can be seen that the calculated scattering profile agrees well with the observed one. The q_d peak is ascribed to the characteristic interparticle distance of the dendrimers accommodated in the lattice. (b)The real-space model constructed for calculating the SAXS profile of the $TETRA_h$ phase using the Debye equation. DNA superhelices are represented by the right-handed helical cylinders with a diameter of 2 nm. The G4 dendrimer molecules are placed in the tunnel regions between DNAs. The helical trajectories of all DNA superhelices in the model are in phase.

The Debye equation was also employed to calculate the SAXS curve associated with the $TETRA_h$ phase. We assumed that all DNA superhelices were right-handed and their helical trajectories were all in phase in the real-space model, as schematically illustrated in Fig. 3(b). The lattice parameters $a = b = 4.08$ nm/$c = 5.1$ nm and P and R_h of the DNA superhelix of 5.4 nm and 0.5 nm, respectively, were used for the calculation. It should be noted that the q_d peak could not be indexed according to the $P4_12_12$ space group; it was hence attributed to the average interparticle distance ($\sim$4.5 nm) of the dendrimers accommodated in the lattice. Consequently, the dendrimer molecules were also incorporated into the real-space model for calculating the SAXS profile, as demonstrated in Fig. 3(b). Fig. 3(a) compares the calculated scattering curve with a representative observed SAXS profile. It can be seen that the agreement was good. The R_h of the DNA superhelices in the $TETRA_h$ phase (*ca.* 0.5 nm) was obviously smaller than that (*ca.* 1.3 nm) associated with the HEX^h phase, confirming that the bending of DNA was weak in the former.

A previous study of the G6 dendriplex by Dootz *et al.* has identified a 3D ordered body-centered orthorhombic structure[36] wherein the DNA was proposed to adopt a curved conformation. This finding along with ours demonstrated that the dendrimers of intermediate generation (G4–G6) are effective structure-directing agents to induce regular and cooperative bending of DNA *via* electrostatic interaction to yield a special class of DNA liquid crystals in which DNA adopts a superhelical conformation with distinct bending states. We call this phenomenon "dendrimer-induced DNA superhelicity". An important property influencing the minimum free energy structure of DNA is its microscopic structural properties. Free B-form DNA in the solution state is often considered as a charged semi-flexible chain; such a model properly describes the thermally averaged conformation of DNA, although it cannot describe the static equilibrium properties accurately.[40] The break down is due to the anisotropic bending potential which arises from the increased flexibility in the direction of the major and minor grooves.[41] DNA possesses a double helical structure in which the major and minor grooves repeat at a distance of 3.4 nm along the chain, resulting in DNA inherently favoring the superhelix formation.[41] Such a phenomenon can indeed be observed in the formation of the nucleosome core particle where DNA wraps around the histone octomer forming a superhelix.[42]

The degree of bending of DNA observed here can be rationalized by the interplay between the bending energy cost of DNA and the free energy of the electrostatic interaction between the DNA and dendrimer.[33] In the case of the dendriplex with a HCl-protonated G4 dendrimer with $(N/P)_n = 6.0$, the driving force of charge matching at a low dendrimer dp (dp $\leq$ 0.2) was not sufficiently strong to outweigh the bending energy cost, so that the DNA chains remained locally straight and packed in a square lattice for maximizing the charge matching with the dendrimer.[35] As the dendrimer dp was increased to the intermediate value (0.22 $<$ dp $\leq$ 0.4), the stronger electrostatic interaction drove DNA to bend slightly into a superhelix while still organized in a tetragonal lattice. The bending of DNA became strong as the dendrimer charge density was further increased (0.5 $\leq$ dp $<$ 0.6), but the DNA superhelices thus formed tended to organize in a hexagonal lattice. The reason why a hexagonal lattice was favored over a tetragonal lattice was likely due to the need for alleviating the local steric repulsion between the DNA superhelices which became strong at large R_h. As demonstrated in our previous study,[43] the hexagonal lattice in which DNA packed in three-fold symmetry contains more water space than the tetragonal lattice, such that DNA organized in the hexagonal lattice suffers from weaker steric repulsion. It is noted that when the dendrimer dp was increased above 0.5, the DNA even wrapped around the dendrimer to form a nucleosome-like structure, but the chromatin-like fibers did not pack into any

Published on 05 July 2021. Downloaded by National Synchrotron Radiation Research on 2/16/2022 7:10:11 AM.

long-range ordered lattice. It should be noted that the analysis of the powder scattering patterns collected in the present study was unable to distinguish the handedness of the DNA superhelices. We postulated that the DNA exhibited slightly anisotropic bending due to the presence of grooves. If the dendrimer bounds around the grooves, then right-handed superhelices would be expected, as that assumed in the real-space models in Fig. 2(a) and 3(b).

In addition to identifying the three types of DNA mesophases, Fig. 1 also reveals the effect of the counterion valency of the protonic acid on the structure of the dendriplex, where the counterions were Cl^-, SO_4^{2-} and PO_4^{3-} for hydrochloric acid, sulfuric acid, and phosphoric acid, respectively. Fig. 1(b) displays the SAXS profiles of the dendriplexes prepared with H_2SO_4-protonated dendrimers as a function of dendrimer dp. It can be seen that the transitions from SQ to $TETRA_h$ and from $TETRA_h$ to HEX_h were deferred to dp = 0.3 and 0.6, respectively, compared to the corresponding transition points (dp = 0.23 and 0.6, respectively) of the dendriplexes prepared with HCl-protonated dendrimers. The dp of the SQ-$TETRA_h$ transition further increased to 0.4 and HEX_h was no longer accessible at dp $\leq$ 0.9 in the dendriplexes prepared using H_sPO_4-protonated dendrimers, as shown in Fig. 1(c). The results clearly showed that the mesomorphic structure with a higher DNA curvature was more difficult to access in the dendriplex with the dendrimer protonated by the multivalent acids compared to the system using monovalent acid as the protonation agent. Nevertheless, the phase transition sequence with respect to the change of dendrimer dp was the same; that is, increasing dp under a fixed $(N/P)_n$ tended to favor the formation of the structure with a higher DNA curvature for enhancing charge matching.

The effect of valency can be understood by considering the entropic gain from counterion release upon the formation of a dendriplex. Under a given dp, the total number of SO_4^{2-} counterions on the dendrimer was half that of the Cl^- counterions when HCl was used for protonation. The smaller number of counterions released to the bulk upon charge matching led to a smaller entropic gain from the counterion release. Moreover, the electrostatic attraction between the multivalent counterions (*i.e.* SO_4^{2-} and PO_4^{3-}) and the ammonium groups on the dendrimer was stronger than that associated with the monovalent counterions. The stronger electrostatic attraction further decreased the amount of free energy reduction arising from the electrostatic interaction energy upon the charge matching between the DNA phosphate group and dendrimer ammonium group. In other words, the combined free energy reduction associated with the counterion release and electrostatic attraction on forming the dendriplexes using multivalent acid-protonated dendrimers was less dominant over DNA bending energy; as a result, it became more difficult to access the structure with more curved DNA.

Conclusions

Cationic PAMAM G4 dendrimers bent DNA into a superhelix in their electrostatic complexes, with the degree of bending increasing with the increase of the dendrimer charge density. While DNA eventually wrapped around the dendrimer with a high charge density (dp $>$ 0.5), two types of superhelical DNA mesophases, in which the DNA superhelices organized in well-defined lattices, were identified at a lower dendrimer charge density. The first type was 3D ordered with a $P4_12_12$ symmetry, where the weakly bent DNA superhelices with $R_h \approx 0.5$ nm and $P \approx 5.1$ nm organized in a tetragonal lattice in which their helical trajectories aligned in phase in the unit cell. The other type developed at a higher dendrimer charge density was 2D ordered, where the strongly bent superhelices with $R_h \approx 1.3$ nm and $P \approx 4.0$ nm packed in the 2D hexagonal lattice without long-range coherence of helical trajectory. The phase windows of the superhelical DNA mesophases depended strongly on the counterion valency of the protonic acid that is used to charge the dendrimer. The threshold dendrimer charge density over which the dendriplex developed the superhelical DNA mesophase increased with an increasing valency of the anionic counterion, which was attributable to the increase of electrostatic attraction of the condensed counterion on the dendrimer and the lower entropic gain from counterion release upon the formation of the dendriplex.

Conflicts of interest

There are no conflicts to declare.

Acknowledgements

This work was supported by the Ministry of Science and Technology, Taiwan, under grant No. MOST 105-2221-E-007-137-MY3. We are indebted to the National Synchrotron Radiation Research Center (NSRRC) for synchrotron beamtime.

References

1 D. Philp and J. F. Stoddart, *Angew. Chem., Int. Ed. Engl.*, 1996, **35**, 1154–1196.
2 M. Muthukumar, *Macromolecules*, 2017, **50**, 9528–9560.
3 B. W. Mansel and H. L. Chen, *Curr. Med. Chem.*, 2020, DOI: 10.2174/0929867327666200728140243.
4 A. M. Carnerup, M. L. Ainalem, V. Alfredsson and T. Nylander, *Soft Matter*, 2011, **7**, 760–768.
5 T. E. Cloutier and J. Widom, *Proc. Natl. Acad. Sci. U. S. A.*, 2005, **102**, 3645–3650.
6 P. Wiggins, T. van der Heijden, F. Moreno-Herrero, A. Spakowitz, R. Phillips, J. Widom, C. Dekker and P. C. Nelson, *Nat. Nanotechnol.*, 2006, **1**, 137–141.
7 R. E. Franklin and R. G. Gosling, *Acta Crystallogr.*, 1953, **6**, 673–677.
8 J. D. Watson and F. H. C. Crick, *Nature*, 1953, **4356**, 738.
9 R. E. Franklin and R. G. Gosling, *Nature*, 1953, **171**, 740–741.
10 Y. Chen, W. Sun, C. Yang and Z. Zhu, *ACS Appl. Bio Mater.*, 2020, **3**, 2805–2815.
11 E. Winfree, F. Liu, L. A. Wenzler and N. C. Seeman, *Nature*, 1998, **394**, 539–544.

 This journal is © The Royal Society of Chemistry 2021

Published on 05 July 2021. Downloaded by National Synchrotron Radiation Research on 2/16/2022 7:10:11 AM.

12 S. M. Douglas, H. Dietz, T. Liedl, B. Högberg, F. Graf and W. M. Shih, *Nature*, 2009, **459**, 414–418.
13 R. Levicky, T. M. Herne, M. J. Tarlov and S. K. Satija, *J. Am. Chem. Soc.*, 1998, **120**, 9787–9792.
14 Y. He, T. Ye, M. Su, C. Zhang, A. E. Ribbe, W. Jiang and C. Mao, *Nature*, 2008, **452**, 198–201.
15 Y. Shao, H. Jia, T. Cao and D. Liu, *Acc. Chem. Res.*, 2017, **50**, 659–668.
16 T. Tørring, N. V. Voigt, J. Nangreave, H. Yan and K. V. Gothelf, *Chem. Soc. Rev.*, 2011, **40**, 5636–5646.
17 T. C. Bishop, *Biophys. J.*, 2008, **95**, 1007–1017.
18 V. A. Bloomfield, *Biopolymers*, 1997, **44**, 269–282.
19 L. C. Gosule and J. A. Schellman, *J. Mol. Biol.*, 1978, **121**, 311–326.
20 L. Naldini, *Nature*, 2015, **526**, 351–360.
21 V. A. Bloomfield, *Curr. Opin. Struct. Biol.*, 1996, **6**, 334–341.
22 C. W. Tabor and H. Tabor, *Annu. Rev. Biochem.*, 1976, **45**, 285–306.
23 N. V. Hud and K. H. Downing, *Proc. Natl. Acad. Sci. U. S. A.*, 2001, **98**, 14925–14930.
24 N. V. Hud, *Biophys. J.*, 1995, **69**, 1355–1362.
25 W. H. Roos, I. L. Ivanovska, A. Evilevitch and G. J. L. Wuite, *Cell. Mol. Life Sci.*, 2007, **64**, 1484–1497.
26 J. C. Wang, *J. Cell Sci., Suppl.*, 1984, **1**, 21–29.
27 K. Drlica, *Mol. Microbiol.*, 1992, **6**, 425–433.
28 K. Fant, E. K. Esbjörner, P. Lincoln and B. Nordén, *Biochemistry*, 2008, **47**, 1732–1740.
29 K. Zhang, M. Jiang and D. Chen, *Angew. Chem., Int. Ed.*, 2012, **51**, 8744–8747.
30 D. A. Tomalia, H. Baker, J. Dewald, M. Hall, G. Kallos, S. Martin, J. Roeck, J. Ryder and P. Smith, *Polym. J.*, 1985, **17**, 117–132.
31 C. J. Su, C. Y. Chen, M. C. Lin, H. L. Chen, H. Iwase, S. Koizumi and T. Hashimoto, *Macromolecules*, 2012, **45**, 5208–5217.
32 Y. C. Huang, C. J. Su, C. Y. Chen, H. L. Chen, U. S. Jeng, N. V. Berezhnoy, L. Nordenskiöld and V. A. Ivanov, *Macromolecules*, 2016, **49**, 4277–4285.
33 C. Y. Chen, C. J. Su, S. F. Peng, H. L. Chen and H. W. Sung, *Soft Matter*, 2011, **7**, 61–63.
34 C. C. Yang, Y. C. Huang, C. Y. Chen, C. J. Su, H. L. Chen and V. A. Ivanov, *Macromolecules*, 2014, **47**, 3117–3127.
35 C. J. Su, H. L. Chen, M. C. Wei, S. F. Peng, H. W. Sung and V. A. Ivanov, *Biomacromolecules*, 2009, **10**, 773–783.
36 R. Dootz, A. C. Toma and T. Pfohl, *Soft Matter*, 2011, **7**, 8343–8351.
37 P. Debye, *Ann. Phys.*, 1915, **46**, 809–823.
38 L. Gelisio and P. Scardi, *Acta Crystallogr., Sect. A*, 2016, **72**, 608–620.
39 R. Gautier and K. R. Poeppelmeier, *Crystals*, 2016, **6**, 3–8.
40 J. A. Schellman, *Biophys. Chem.*, 1980, **11**, 321–328.
41 A. A. Travers, *Philos. Trans. R. Soc., A*, 2004, **362**, 1423–1438.
42 V. B. Zhurkin, Y. P. Lysov and V. I. Ivanov, *Nucleic Acids Res.*, 1979, **6**, 1081–1096.
43 Y. C. Liu, H. L. Chen, C. J. Su, H. K. Lin, W. L. Liu and U. S. Jeng, *Macromolecules*, 2005, **38**, 9434–9440.